Journal of Power Sources 200 (2012) 67–76

Contents lists available at SciVerse ScienceDirect

Journal of Power Sources

journal homepage: www.elsevier.com/locate/jpowsour

Towards the understanding of coatings on rate performance of $LiFePO_4$

Jin Chong[a,b], Shidi Xun[a,*], Xiangyun Song[a], Paul Ridgway[a], Gao Liu[a], Vincent S. Battaglia[a]

[a] Lawrence Berkeley National Laboratory, Berkeley, CA 94720, USA
[b] Tianjin Institute of Power Sources, Tianjin 300381, China

ARTICLE INFO

Article history:
Received 19 August 2011
Received in revised form 19 October 2011
Accepted 19 October 2011
Available online 25 October 2011

Keywords:
$LiFePO_4$
Carbon coating
$Li_4P_2O_7$ coating
Electronic conductivity
Li^+ diffusion
Lithium ion batteries

ABSTRACT

Stoichiometric and non-stoichiometric $LiFePO_4$ nanoparticles (sub 100 nm) were synthesized and compared to carbon coated $LiFePO_4$ particles (super 100 nm) of similar electrode composition for rate performance. The materials were characterized by X-ray diffraction (XRD) and high resolution transition electron microscopy (HRTEM) where amorphous layers (<5 nm) were observed on both the non-stoichiometric and carbon-coated $LiFePO_4$ primary particles. Secondary particles of stoichiometric and non-stoichiometric sub 100 nm particles were confirmed by TEM and scanning electron microscopy (SEM). All three materials display similar particle size distributions as measured with a particle size analyzer and an SEM, indicating that the sub 100 nm particles form secondary particles of approximately the same size as the carbon coated super 100 nm particles. The electronic conductivity measurements of each material indicate that the non-stoichiometric $LiFePO_4$ measures between 4.5×10^{-5} and 2.18×10^{-4} S cm^{-1}, 8 orders of magnitude lower than the conductivity of the carbon coated super 100 nm $LiFePO_4$. Rate tests of the electrodes demonstrate faster charge and discharge capability as the level of conductive additive in the electrodes approaches 15 wt%. All three materials demonstrate solid state diffusion limitations: electrodes of the non-stoichiometric and the carbon coated material both show extreme high rate performance with the addition of 15% carbon additive. A simple calculation indicates that this is the level of carbon additive needed to completely coat particles of 100 nm in size.

Published by Elsevier B.V.

1. Introduction

Lithium rechargeable batteries are today's best energy storage option for electric vehicles (EVs). Top candidates among the many Li-ion technologies must demonstrate good safety, low price, long calendar and cycle life, and high energy density. Among the cathode materials, $LiFePO_4$ has attracted considerable attention due to its potential for low cost, good cycleability, and high thermal stability. The intrinsic limitations of $LiFePO_4$ are its low electronic and Li transport properties resulting in poor rate capability [1,2]; however, $LiFePO_4$ can be engineered to charge and discharge quickly. One method to improve the rate performance is to carbon coat the $LiFePO_4$ particles by pyrolyzing them with a carbon-containing compound at *ca.* 700 °C [3]. C/$LiFePO_4$ composites (15 wt% carbon) made by mixing the initial precursors to $LiFePO_4$ with a carbon gel shows a capacity of about 120 mAh g^{-1} when discharged at 5 C_{10} [4]. Some attempts have been made to reduce the carbon content of C/$LiFePO_4$-based electrodes in order to increase the specific energy and energy density [5]. By employing this strategy, $LiFePO_4$ with a 3.2 wt% carbon coating corresponding to a coating thickness of 1–2 nm has been prepared [6]. The composite electrode delivered 80% of its theoretical capacity at a current density of 170 mAh. Decreasing the particle size to nanoscale is another approach to improving the rate capability of $LiFePO_4$. Thus, a molten salt casting method was investigated to synthesize $LiFePO_4$, by which the particle size could be controlled down to 25 nm [7]. These particles tend to agglomerate to form secondary particles with a size on the order of 100 nm. With 2 wt% carbon additive, capacities of 157 mAh g^{-1} and 108 mAh g^{-1} were obtained at C_{10}/10 and 10 C_{10}, respectively.

Beyond a simple carbon coating, $LiFePO_4$ co-coated with carbon and oxides have been explored. A CuO and carbon co-coated $LiFePO_4$ composite was prepared with the objective of filling in the incomplete carbon network covering the particles with nanosized CuO [8]; however, only 125 mAh g^{-1} of discharge capacity was obtainable by this method. ZnO and carbon co-coating has also been investigated but with limited success [9]. In addition, pure oxides have been evaluated; the effects of a TiO_2 coating on cycle performance of an $LiFePO_4$ cathode cycled at 55 °C against Li or C (mesocarbon microbeads) anodes was investigated [10]. It was found that the TiO_2 coating imposed a deteriorating effect on the C/$LiFePO_4$ cell. $LiFePO_4$ with 2–3 nm of a ZrO_2 layer was prepared by a chemical precipitation method [11]. 100 mAh g^{-1} of discharge capacity was achieved at 1 C_{10}. Other coatings, such as AlF_3 [12] and NiP [13], have also been studied, indicating that they cannot improve the rate performance efficiently.

* Corresponding author. Tel.: +1 5104867172; fax: +1 510 4864260.
E-mail address: sxun@lbl.gov (S. Xun).

0378-7753/$ – see front matter. Published by Elsevier B.V.
doi:10.1016/j.jpowsour.2011.10.073

One of the most acclaimed and disputed materials is the $Li_4P_2O_7$ coated $LiFePO_4$ reported by Ceder [14–16], which is also referred to as non-stoichiometric $LiFe_{0.9}P_{0.95}O_{4-\delta}$ [14]. The $LiFe_{0.9}P_{0.95}O_{4-\delta}$ primary particles are less than 50 nm in diameter with an amorphous coating layer thickness less than 5 nm. The $LiFe_{0.9}P_{0.95}O_{4-\delta}$ electrodes (80% active material, 15% super-P carbon black, and 5% polyethylene tetrafluoride (PTFE) binder) were cycled from 2.0 to 4.3 V with a loading density of 2.5–4.0 mg cm^{-2}. 166 mAh g^{-1} discharge capacities could be achieved at a 2 C_{10} discharge rate. Even at a 50 C_{10} rate, the material still delivered 80% of its theoretical capacity (130 mAh g^{-1}). As the amount of conductive additive is increased to 65%, 100 mAh g^{-1} and 60 mAh g^{-1} discharge capacities are obtained at the extremely high rates of 197 C_{10} and 397 C_{10}, respectively. Despite these results, the certainty of the presence of an amorphous $Li_4P_2O_7$ glass phase and its contribution to the rate performance are still under debate [15]. Residual carbon derived from the synthesis process is one source of concern as a possible contributor to the super high-rate [17], another is the possibility of improved ionic conductivity as a result of carbon induced porosity.

Ultimately, coating layer, primary and secondary particle size, amount of conductive additives, active material loading density, and electrode thickness and porosity all influence an electrode's rate performance. Moreover, the type of binder and electrode preparation also can have a significant influence. The rate performance of the $LiFe_{0.9}P_{0.95}O_{4-\delta}$-based electrodes as initially published showed the super high-rate performance as the carbon additive content increased to greater than 30% [14], a design not typically used in commercial electrodes but used to prove the authors' premise that $LiFePO_4$ is not inherently slow. In this study, carbon coated $LiFePO_4$ from Hydro Quebec and $LiFe_{0.9}P_{0.95}O_{4-\delta}$, prepared as dictated by Ceder's group, were tested under the same conditions to identify the effects of different types of coating layer, different amounts of conductive carbon black additive, and different active material loading densities on the $LiFePO_4$'s overall rate performance. A stoichiometric nano-material prepared the same way as the non-stoichiometric material was also part of the comparison.

2. Experimental

$LiFe_{0.9}P_{0.95}O_{4-\delta}$ was synthesized by a solid-state reaction using Li_2CO_3 (99.0%, Alfa Aesar), $FeC_2O_4{\cdot}2H_2O$ (99.999%, Alfa Aesar), and $NH_4H_2PO_4$ (98.0%, Alfa Aesar), according to the method reported [14]. Stoichiometric $LiFePO_4$ was prepared by the same procedure but with stoichiometric amounts of the precursors. The mixture in the acetone was ball-milled and heated at 350 °C for 10 h under argon to decompose the carbonate, oxalate and ammonium. The sample was cooled to room temperature, ground and manually pelletized under 50 kN cm^{-2} pressure using a disk-shaped die. After preheating, the pellet was heated at 600 °C for 10 h under argon. Carbon coated $LiFePO_4$ was obtained from the Institute de Recherché d'Hydro-Québec (IREQ). A slurry casting method has been developed by this lab and used to prepare all of the electrodes [18]. Battery grade acetylene black (AB) was acquired from Denka Singapore Private Limited. Polyvinylidene difluoride (PVDF) no. 1100 binder was purchased from Kureha, Japan. Anhydrous *N*-methylpyrrolidone (NMP) was purchased from Sigma–Aldrich. Electrode slurries were made by mixing active material, AB, and PVDF binder in anhydrous NMP solvent. Additional amounts of NMP solvent were added to give the mixture an "appropriate" viscosity. The mixture was blended together using a Polytron PT 10-35 homogenizer at 3000 rpm until uniform (about 10 min). The slurries were coated on aluminum current collector by using a doctor-blade. Different loading densities of electrodes were cast by controlling the height of the doctor-blade. After the NMP evaporated, the dry laminates were calendared to 30% porosity. The calendared laminates were then punched into 1.27 cm diameter electrodes. The punched electrodes were dried under vacuum at 140 °C for 16 h and then transferred into an argon atmosphere glove box. Electrodes containing 87.2% active material, 4.8% AB, and 8.0% PVDF were tested from C_{10}/10 to 60 C_{10}; electrodes containing 80% active material, 15% AB, and 5% PVDF were tested from C_{10}/10 to 100 C_{10}; and electrodes containing 30% active material, 65% AB, and 5% PVDF were tested from C_{10}/10 to 600 C_{10}. To obtain a robust laminate containing 65% AB, the AB must first undergo ball-milling to *ca.* 30% of its original volume before addition to the slurry.

For electrochemical measurements, an electrolyte of 1 M $LiPF_6$ in EC:DEC (1:1 by mass) was used in each of the cells. The charge-discharge tests were performed in CR2325 coin cell hardware with Li counter electrodes and Celgard 2500 separators. The cells were charged under CCCV mode and discharged under CC mode. The charge current used for each sample was the same as the discharge current plus a voltage hold at 4.3 V until the current fell below C_{10}/100 mA, and then discharged to 2.5 V. All of the cell measurements were performed with a Maccor 4000 battery tester at 30 ± 2 °C in an environmental chamber from Testequity (model TEC1).

The 200 kV FEI monochromatic F20 UT Tecnai was used to produce high resolution TEM images of the powders. The phase of powders was identified by a Philips X'Pert Pro Multipurpose X-ray Diffractometer using Cu Kα radiation (λ = 0.15406 nm). The morphology of electrodes was imaged with a JEOL JSM-7500F field emission scanning electron microscope (SEM). The powder specific surface area was measured by the Brunauer–Emment–Teller (BET) N_2 adsorption method with a Micromeritics Tristar surface area and porosity analyzer. Particle size distribution was measured with an LS230 particle characterization instrument. The electronic conductivity measurements were performed using the four-point-probe D.C. method with a Solartron 1286 Electrochemical Interface analyzer and CorrWare software under Galvanoatatic mode [19]. The measurements were conducted on pellets, which were fabricated under different hydrostatics pressures in a 13 mm diameter die. The pellets were sintered in a furnace at 600 °C for 10 h under an inert atmosphere (argon) in order to desensitize them [19]. The conductivity of each pellet was measured three times at different locations on the pellet to assess the average value and the variability. All of the conductivity tests were performed at room temperature (*ca.* 23 °C).

3. Results and discussion

3.1. Physical characterization

Fig. 1 shows the SEM images of $LiFe_{0.9}P_{0.95}O_{4-\delta}$, stoichiometric $LiFePO_4$, and C/$LiFePO_4$ materials. All three material particle sizes are on the order of 100 nm. For the non-stoichiometric and stoichiometric materials, the particles are secondary particles whereas the C/$LiFePO_4$ particles are primary particles. Fig. 2 shows the XRD patterns of $LiFe_{0.9}P_{0.95}O_{4-\delta}$, stoichiometric $LiFePO_4$, and C/$LiFePO_4$ along with the standard $LiFePO_4$ spectrum for comparison. The three powders display nearly the same XRD patterns. No carbon can be identified in the spectrums, even for the carbon coated material, which contains less than 3.5% carbon [5–7,20]. In addition, no crystalline $Li_4P_2O_7$ or Li_3PO_4 phase is identifiable from 20° to 32° (Fig. 2b) in the non-stoichiometric phase. As reported, very weak $Li_4P_2O_7$ and Li_3PO_4 phase peaks were found for $LiFe_{0.9}P_{0.95}O_{4-\delta}$ when sintered to 800 °C [14]; however, there were no corresponding peaks observed here (Fig. 2c). The difficulty in finding $Li_4P_2O_7$ with XRD is due to its low content and its amorphous structure. Also, the $Li_4P_2O_7$ peaks, if present, could be shielded by background noise.

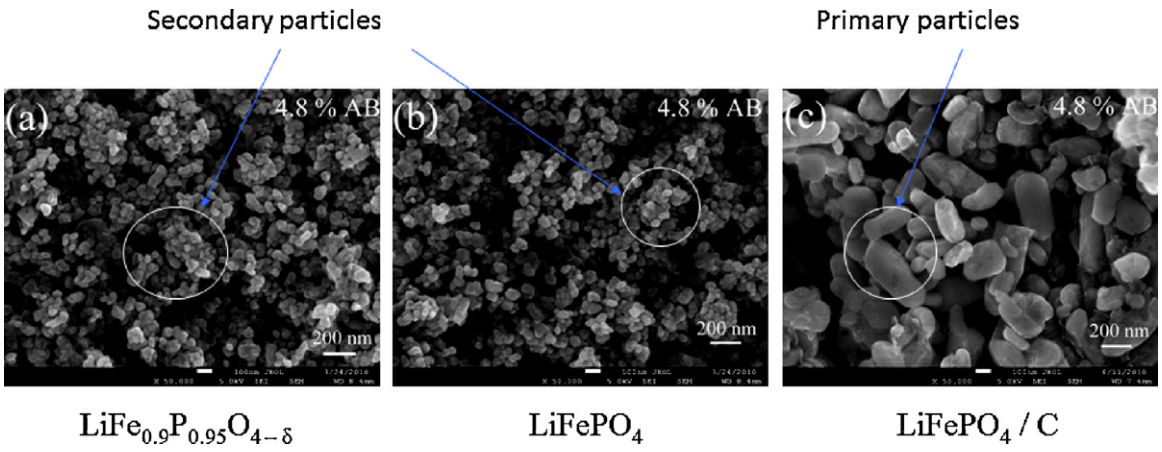

Fig. 1. The SEM images of $LiFe_{0.9}P_{0.95}O_{4-\delta}$, stoichiometric $LiFePO_4$, and C/$LiFePO_4$ materials.

TEM was employed to observe the fine structure of the $LiFePO_4$ particles. A 3–4 nm thick amorphous layer was observed for the $LiFe_{0.9}P_{0.95}O_{4-\delta}$ as seen in Fig. 3a. Comparatively, no obvious coating layer was observed on the stoichiometric $LiFePO_4$ material, although a slightly disordered amorphous film can be seen due to the uncompleted crystallization along the primary particles' boundaries (Fig. 3b), which is common for this material [7]. Fig. 3c shows the TEM image of C/$LiFePO_4$; an amorphous layer is visible on the $LiFePO_4$ particles with a thickness less than 5 nm. Moreover, the primary particles of $LiFe_{0.9}P_{0.95}O_{4-\delta}$ and stoichiometric $LiFePO_4$ identified in Fig. 3(a) and (b) are seen to be tightly packed together. Evidently, the primary, nano-sized particles fuse together during the sintering step of the synthesis process. This point will be referred to later when discussing the rate capability. For the C/$LiFePO_4$, just as in the SEM, no secondary particles were observed (Fig. 3c).

The particle size and distribution were measured by BET and PSA analysis, respectively. BET surface area for $LiFe_{0.9}P_{0.95}O_{4-\delta}$, stoichiometric $LiFePO_4$, and C/$LiFePO_4$ were measured at 33.96, 47.32, and 12.93 $m^2\,g^{-1}$, respectively. If one assumes the particles are spherical and substitutes the BET surface area into the equation

$$d = \frac{6}{\rho a}$$

one can solve for the average particle diameter d, where ρ is the material density in grams per cm^3 and a is the BET measured surface area in m^2 per gram. Substitution of these values assuming a

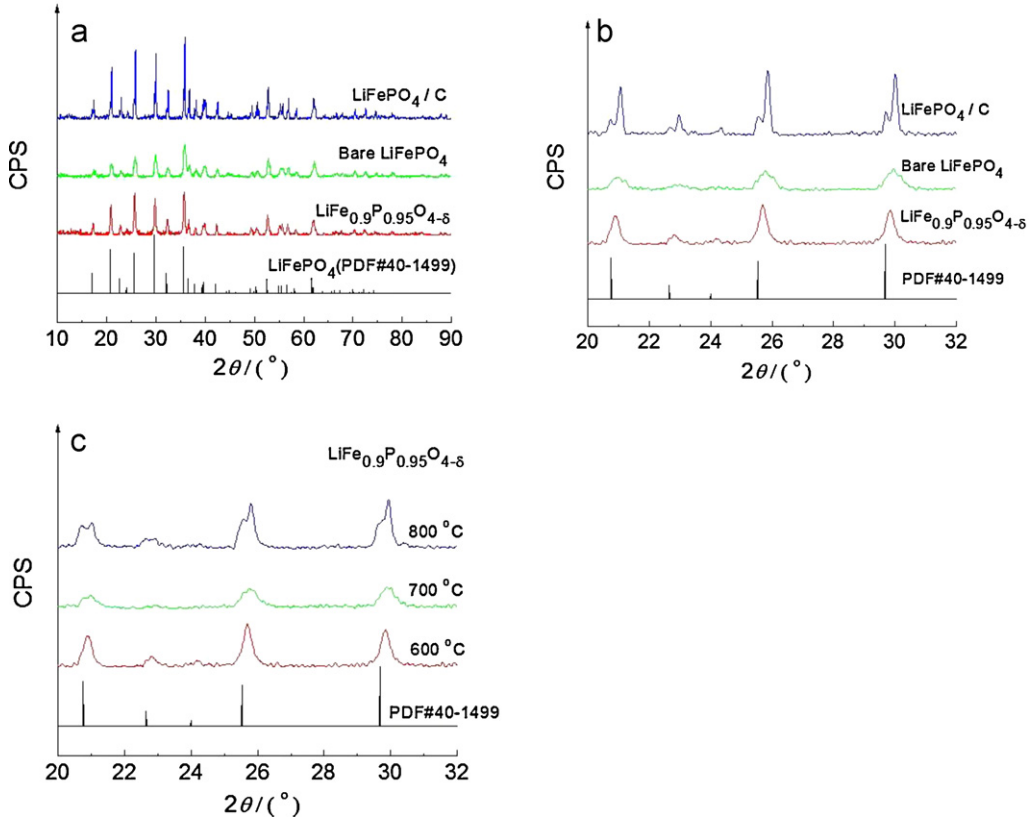

Fig. 2. XRD patterns of (a) $LiFe_{0.9}P_{0.95}O_{4-\delta}$, stoichiometric $LiFePO_4$, and C/$LiFePO_4$ powders (sintered at 600 °C); (b) enlargement of (a) between 20 and 32°; (c) same 2 range but for $LiFe_{0.9}P_{0.95}O_{4-\delta}$ sintered at different temperatures.

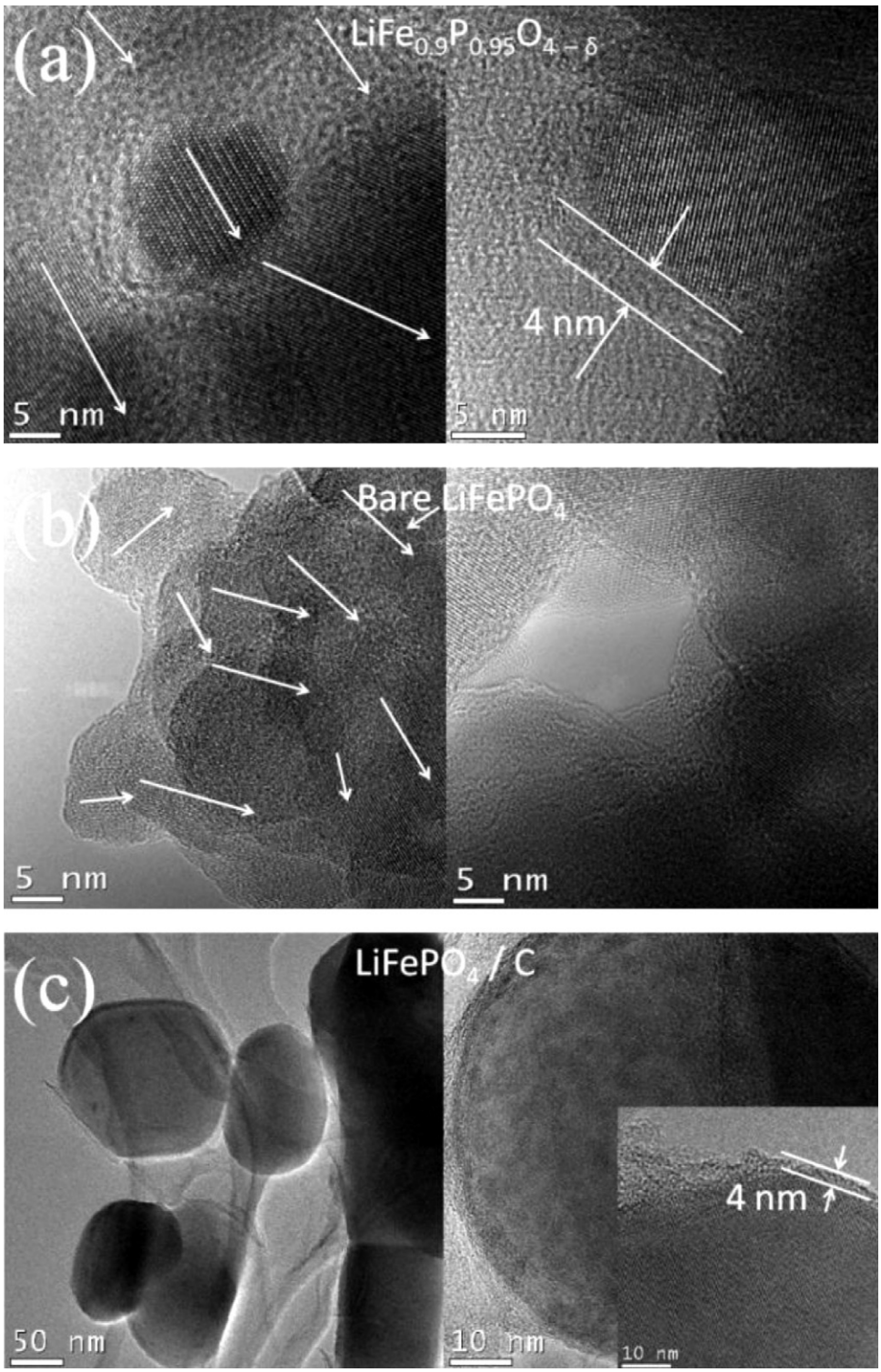

Fig. 3. TEM images of (a) $LiFe_{0.9}P_{0.95}O_{4-\delta}$; (b) stoichiometric $LiFePO_4$; and (c) C/$LiFePO_4$. (The arrows in (a) and (b) point to grain boundaries between secondary particles.)

Table 1
Summary of particle size distribution and BET surface area.

Sample	D_{10} (μm)	D_{50} (μm)	D_{90} (μm)	BET ($m^2\ g^{-1}$)
$LiFe_{0.9}P_{0.95}O_{4-\delta}$	0.135	0.333	0.498	33.9551
Stoichiometric $LiFePO_4$	0.219	0.402	0.651	47.3239
C/$LiFePO_4$	0.252	0.415	0.657	12.9335

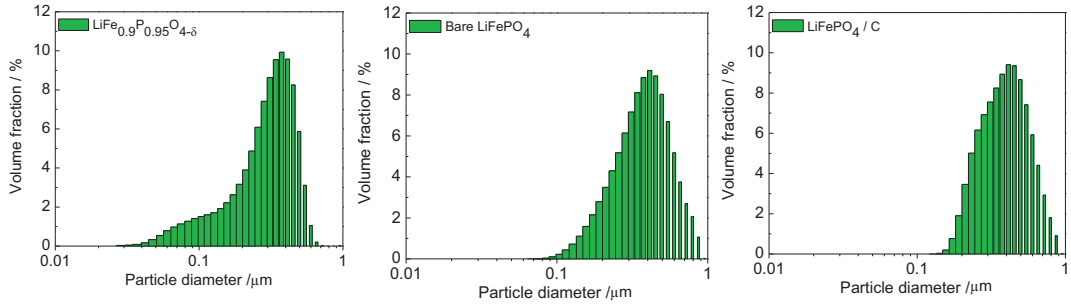

Fig. 4. Particle size distribution of $LiFe_{0.9}P_{0.95}O_{4-\delta}$, stoichiometric $LiFePO_4$ and C/$LiFePO_4$ measured by PSA.

density of 3.6 g cm^{-3} gives average diameters of 32, 44, and 116 nm for the materials, respectively. We saw earlier in the SEMs and TEMs that the primary particles of the secondary particles are on the order of 25 nm, which suggests that the BET is measuring the average particle size of the secondary particles and that the area between the primary particles within a sintered secondary particle is inaccessible to the N_2 gas of the instrument. We have seen for other materials that the BET measurement of secondary particles predicts a particle diameter of roughly 1/3 the size as viewed under SEM (Fig. 1), and has typically been associated with surface roughness of the particles. If this were also to apply here, we would expect particle sizes on the order of 100 nm for all three materials. A PSA was performed on each material, as shown in Fig. 4 and summarized in Table 1. In this instrument, where light scattering is relied upon to determine particle size, the $LiFe_{0.9}P_{0.95}O_{4-\delta}$ and stoichiometric $LiFePO_4$ materials were observed to have a D_{50} of 0.333 μm and 0.402 μm, respectively. Again, even though it is evident from the SEM and TEM that the primary particles are approximately 25 nm in diameter, it is the secondary particle size that is measured by the PSA. The C/$LiFePO_4$ does not form secondary particles and its D_{50} was measured at 0.415 μm. Thus, although the primary particle size for the synthesized materials are nearly the same and are quite smaller than the carbon coated material from IREQ; their secondary particles are very close in size to the primary particles of IREQ. As will be discussed in results below, it is this secondary particle size measured by the BET and PSA that dictates the electrode performance.

Usually, electronic conductivity is very important to the performance of an electrode's active material. In order to assess the electronic properties of the particles, solid pellets of the particles prepared under different pelletizing pressures were measured for their bulk electronic conductivity using a four-point probe. After a sintering step that lasted 10 h at 600 °C, the pellets were allowed to cool and then the conductivity of each pellet was measured three times at different locations on the pellet. The resulting data are shown in Fig. 5 where it can be seen that the conductivities increase slightly with an increase of the pelletization pressure-considered a result of the better particle-to-particle contact as a result of the compression. As one might expect, the C/$LiFePO_4$ has the highest conductivity value of 0.9–3.66 × 10^3 S cm^{-1}, which is the reason why the material was coated in the first place [21]. The electronic conductivity of the solid-state synthesized stoichiometric $LiFePO_4$ was measured in the range of 2.88–5.87 × 10^{-3} S cm^{-1}, which is consistent with the value reported previously [19]. Among the three materials, $LiFe_{0.9}P_{0.95}O_{4-\delta}$ showed the lowest electronic conductivity of 4.5 × 10^{-5}–2.18 × 10^{-4} S cm^{-1}, and proves that the Li–P–O-coating process does not improve the electronic conductivity of $LiFePO_4$ as suspected by some critics of the initial publication. To the contrary, this layer appears to decrease the conductivity as compared with the stoichiometric material synthesized *via* the same process.

3.2. Morphology of electrodes

The electrodes of the $LiFe_{0.9}P_{0.95}O_{4-\delta}$, stoichiometric $LiFePO_4$, and C/$LiFePO_4$ with different amounts of AB additive (4.8%, 15.0%, and 65.0%) were examined by SEM, as shown in Fig. 6. It can be seen from Fig. 6a and b that the electrodes consist of secondary particles on the order of 100 nm in diameter. However, although no secondary particles were observed for the C/$LiFePO_4$ material, the primary particle size is also on the order of 100 nm (as seen in Fig. 6c, f, and i), consistent with the TEM, BET, and PSA observations. The active material and AB can be distinguished from each other in the SEM since the AB is on the order of 40–50 nm and is very conductive, and hence appears darker in the images. Most of the particles observed in the SEMs of the electrodes containing 4.8% AB are of the active material. At 4.8%, there is not enough AB to completely coverall of the active material. The situation changes as the AB content is increased to 15%. When the AB content reaches 65%, all but a few surface particles of the active material are encapsulated by AB. A percolation-tunneling based model has been developed to study the electrical conductivity of a $LiFePO_4$-based composite electrode [22]. The study showed that ultra-fine, carbon-free, nano-sized particles (50 nm) require a relatively large amount of carbon black to increase the electronic conductivity. With improved electronic conductivity, the cell performance can be improved [22].

3.3. Rate performance

As reported, compared with other $LiFePO_4$ materials, $LiFe_{0.9}P_{0.95}O_{4-\delta}$ can be a fast charge and discharge material

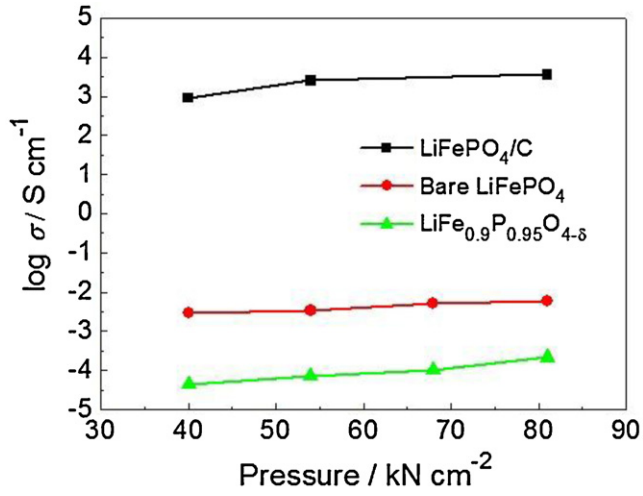

Fig. 5. The electronic conductivity of $LiFe_{0.9}P_{0.95}O_{4-\delta}$, stoichiometric $LiFePO_4$, and C/$LiFePO_4$ materials, measured on pellets compressed under different static pressures.

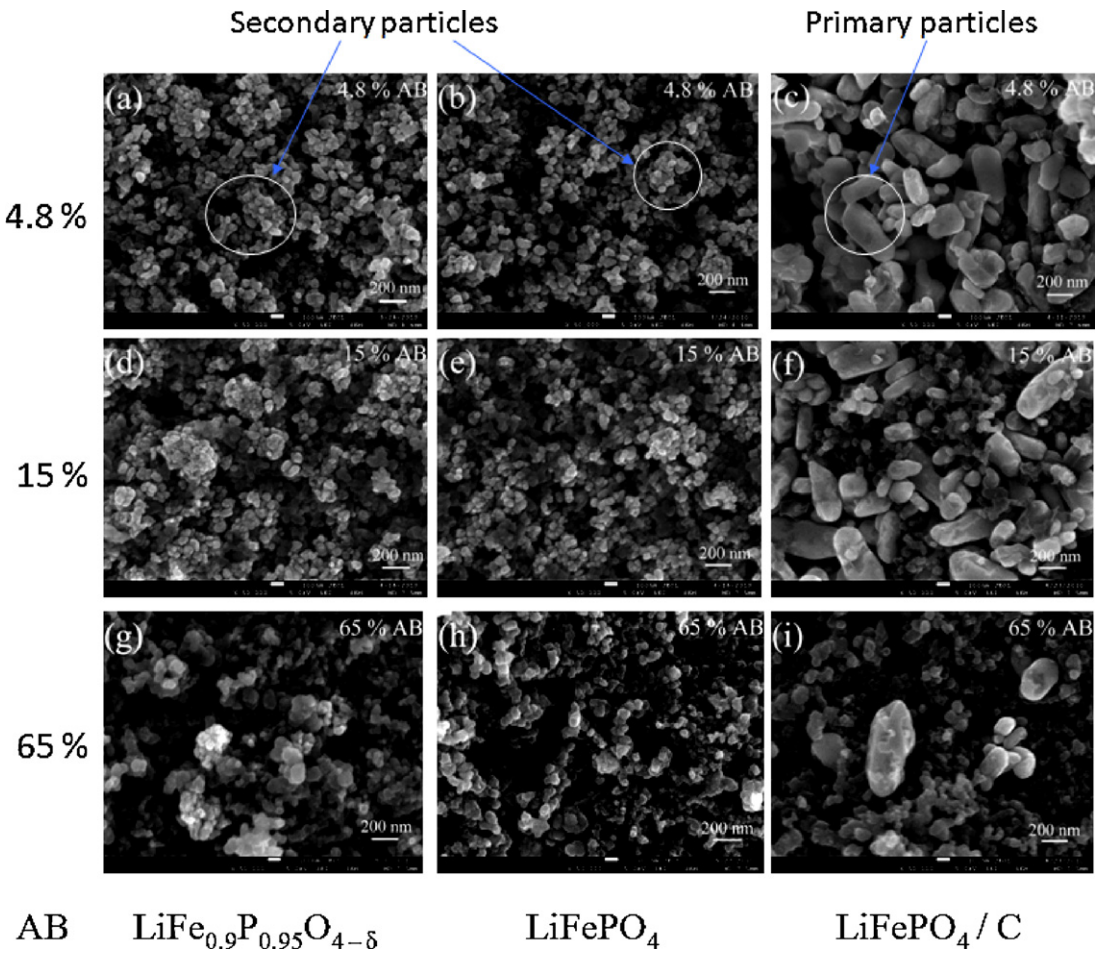

Fig. 6. SEM images of electrodes of different carbon contents: $LiFe_{0.9}P_{0.95}O_{4-\delta}$ (a, d, and g); stoichiometric $LiFePO_4$ (b, e, and h); and C/$LiFePO_4$ (c, f, and i).

with excellent capacity retention [14]. However, this high rate performance required a high AB loading (30–65%), which is not typical of most battery designs but was used in the referenced work as a means of demonstrating the material inherently high rate capability. In this study, the rate performance for all three materials was tested in electrodes of 4.8%, 15%, and 65% AB. Fig. 7 shows their rate performance with the different amounts of conductive AB and different active material loading densities through use of a modified Peukert plot that has been normalized with the discharge capacity measured at C/10 mA (C_{10}). The charge current used for each sample was the same as the previous discharge current for all of the data presented in this figure plus a voltage hold at top of charge at 4.3 V until the current fell below C_{10}/100 mA. As shown, the capacity retention rate with discharge was significantly improved with the increase of conductive additive from 4.8% to 15% for all three materials. Electrodes with 65% carbon additive show the best rate performance for all three active materials, although such improvements were significant only at extremely high rates. All of the data for a particular material overlap at the lower currents with some finite negative curvature, independent of the thickness of the electrodes. The curvature of the Peukert plots, even at low current densities, is indicative of solid-state diffusion limited cells, especially for cells of such low loadings at these. As the rate is increased, the negative curvature of the data belonging to the lowest carbon content electrodes accelerates, separating from the other two curves of the 15 and 65% AB. Electrodes of the stoichiometric nanomaterial and carbon coated material show small improvement in rate as the carbon content was increased from 15% to 65%; there is more of an effect seen with the non-stoichiometric nanomaterial. The thickness of the electrodes does not affect the rate performance at the high AB levels, as can be seen in Fig. 7. The rate curves of electrodes of the same active material but different loadings and containing 65% AB are identical for each of the three materials. This is also consistent with the fact that the electrode performance is limited by the solid state diffusion of the particles and not by the transport properties of the electrolyte.

To understand these results a little better, the voltage *versus* discharge curves at 20 C_{10} for each material and for each carbon contents are plotted in Fig. 8. As a reminder to the reader, the initial drop in voltage at the beginning of discharge (within the first second) can be attributed to a combination of the ohmic resistance and charge transfer resistance in the cell. (The concentration polarization of the salt sets up in the next 10's of seconds.) As the cell continues to discharge, the voltage profile will eventually tail off, mimicking the voltage curve near the end of discharge, and reach the specified cut-off voltage which defines the end of discharge. If this discharge capacity is less than that achieved at lower discharge rates and the ohmic and kinetic resistances not so severe that the cut-off voltage is within a few 100 ms, it is typically due to one of two events: the concentration profile of the salt is such that the back of the electrode and not accessible and hence only a fraction of the electrode is accessed, or the transport of Li^+ in the solid is so slow that the concentration of the lithium on the surface of the material leads to the premature decline of the cell voltage to the cut-off voltage.

To discern whether the sharp voltage drop in the C/$LiFePO_4$ material was due to charge transfer polarization or ohmic

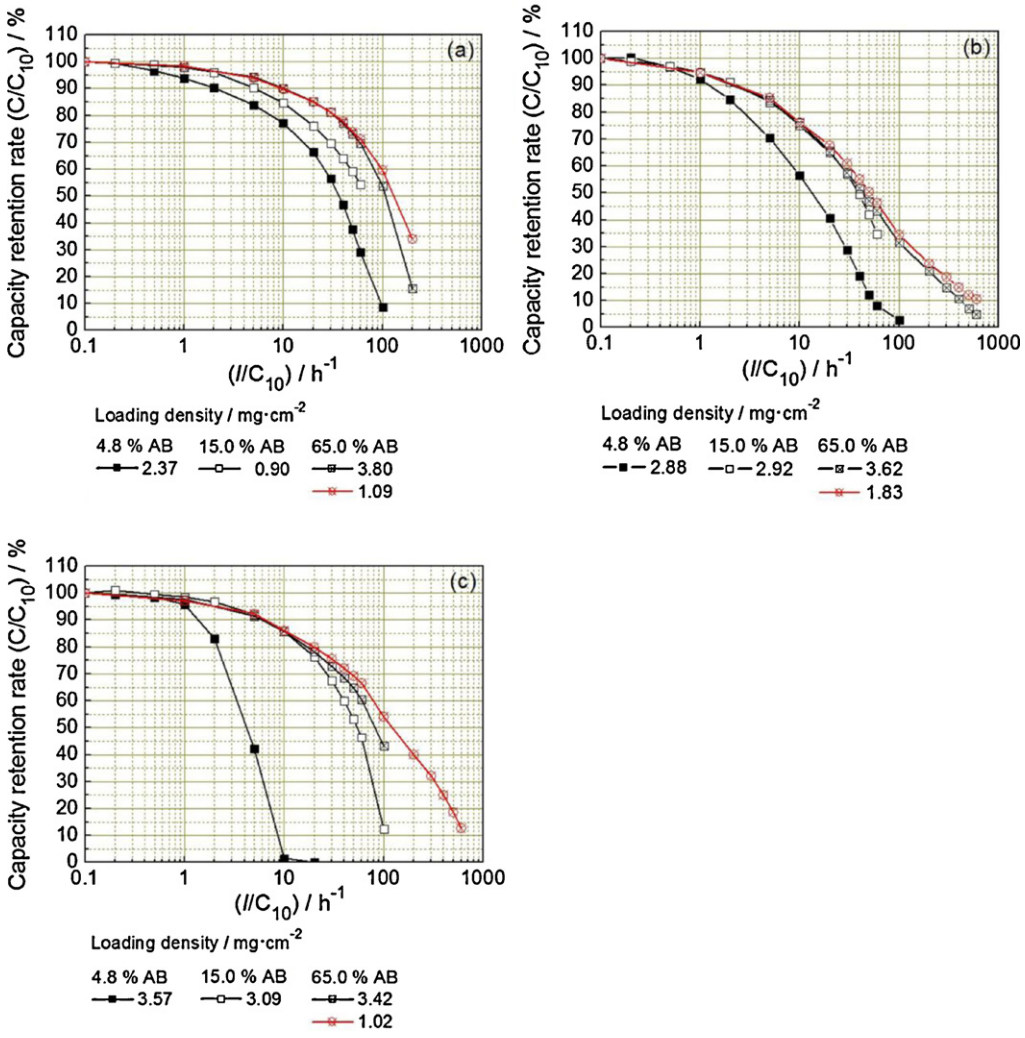

Fig. 7. The rate performance of (a) $LiFe_{0.9}P_{0.95}O_{4-\delta}$, (b) stoichiometric $LiFePO_4$, and (c) C/$LiFePO_4$ electrodes with different amounts of AB and loading densities.

resistance, the following analysis was performed. The Tafel equation takes the form $I = I_0 \exp(\alpha F/RT)\eta$, where I is the current of the cell; I_0 is the electrode's exchange current; α is the charge transfer coefficient, which we set to 0.5; F is the Faraday constant, $F = 96{,}485\,C\,mol^{-1}$; R is the universal gas constant, $R = 8.314\,V\,C\,mol^{-1}\,K^{-1}$; T is the absolute temperature, $T = 303.15\,K$; and η is the electrode overpotential. The equation can be inverted to portray η as a function of current: $\eta = (RT/\alpha F)\ln(|I|/|I_0|)$. The cell polarization can now be written as: $\Delta V = IR_\Omega + \eta = IR_\Omega + (RT/\alpha F)\ln(|I|I_0|)$, where R_Ω is the cell's ohmic resistance and I_0 is the sum of the exchange currents for the cathode and the lithium counter electrode. This equation can be re-arranged to $(\Delta V - (RT/\alpha F)\ln|I|) = IR_\Omega - (RT/\alpha F)\ln|I_0|$. Based on the cell voltage *versus* discharge capacity data of Fig. 9, the initial drop in the discharge voltage for the C/$LiFePO_4$ electrode with 4.8% AB minus the log of the current $(\Delta V - (RT/\alpha F)\ln|I|)$ is plotted *versus* I and plotted in Fig. 10. From this figure, a linear fit to the data gives an intercept that translates to a combined exchange current $I_0 = 9.12\,\mu A$. Accordingly, the calculated electrode exchange currents for the cells with $LiFe_{0.9}P_{0.95}O_{4-\delta}$ and stoichiometric $LiFePO_4$ acquired *via* the same methodology were 68.33 μA and 53.24 μA, respectively. The slope of the linear fit translates to an ohmic resistance of 20.2 Ω, 0.10 Ω and 0.19 Ω for the cells of C/$LiFePO_4$, $LiFe_{0.9}P_{0.95}O_{4-\delta}$, and stoichiometric $LiFePO_4$, respectively. One can substitute these values back into the original expression to calculate the contributions of each to the total voltage drop, as provided in Table 1. From this analysis, we see that both the ohmic and kinetic resistance are large for the cell with C/$LiFePO_4$ and just 4.8% AB and they contribute in near equal proportions to the initial cell impedance at 20 C_{10}. This is enough impedance to cause the voltage to hit the lower cut-off voltage almost immediately.

This result was somewhat unexpected, as the carbon coated powder demonstrated the highest electronic conductivity (Fig. 5). One explanation for this is that charge transfer is limiting the discharge rate and the surface areas of $LiFe_{0.9}P_{0.95}O_{4-\delta}$ and stoichiometric $LiFePO_4$ particles are approximately three times larger than that of C/$LiFePO_4$ (Table 1). In conjunction with this, as the PVDF is known to coat particles, electrodes with lower overall internal surface areas may result in having thicker PVDF coatings on each particle; thus, for the C/$LiFePO_4$, because its surface area is smaller than that of $LiFe_{0.9}P_{0.95}O_{4-\delta}$ and stoichiometric $LiFePO_4$, it is possible that there is more PVDF covering the low surface area C/$LiFePO_4$ particles and the AB. This further reduces the charge transfer capability and electrically isolates the particles. Thus, under the low AB content (4.8%) condition, low surface areas C/$LiFePO_4$ particles are isolated by the thicker, insulating PVDF layer leading to Li^+ and/or electron transport limitations that result in poor overall rate performance.

As the AB content is increased to 15%, the high rate afforded by either coatings is realized, see Fig. 7. At C_{10}/1, the electrodes

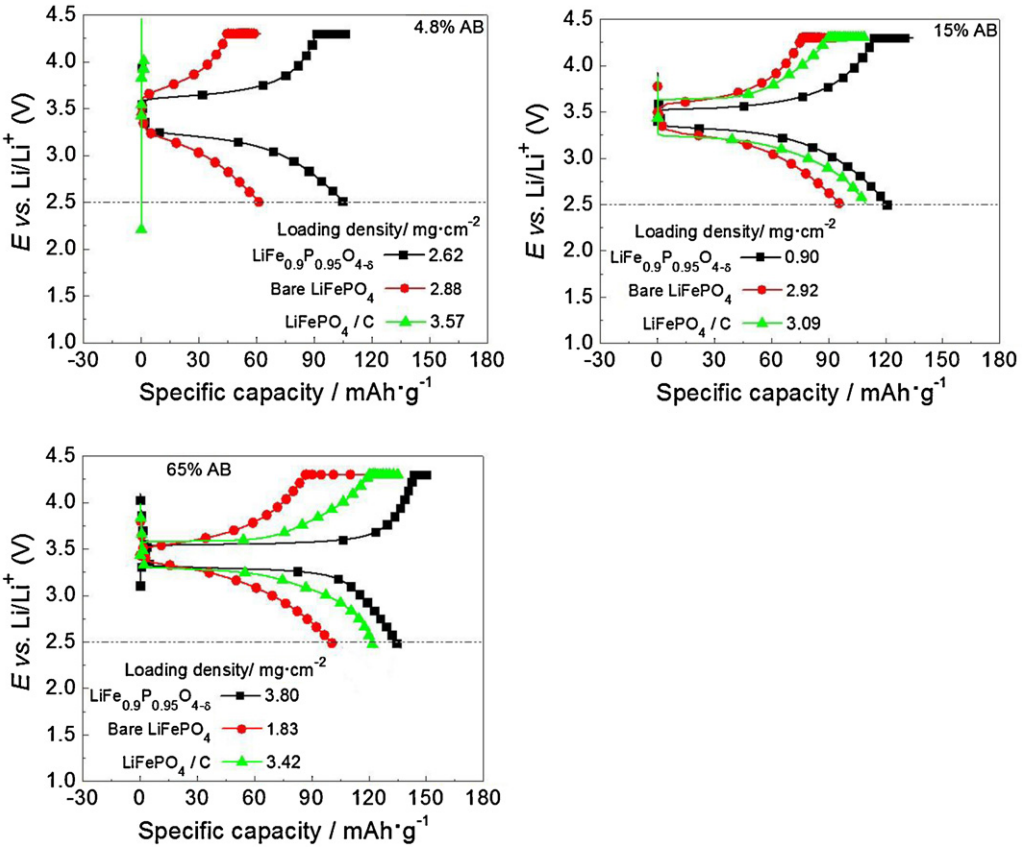

Fig. 8. The potential plots of $LiFe_{0.9}P_{0.95}O_{4-\delta}$, stoichiometric $LiFePO_4$, and C/$LiFePO_4$ with a CCCV charge and CC discharge at 20 C_{10}.

of $LiFe_{0.9}P_{0.95}O_{4-\delta}$ and C/$LiFePO_4$ retain nearly all of the capacity measured at C_{10}/10, whereas, just 95% of the C_{10} capacity is retained for the stoichiometric $LiFePO_4$. As mentioned, for these fairly thin films, the curvature of the lines with high carbon content is reflective of limited solid state diffusion. One can clearly see that this curvature is more pronounced for the stoichiometric $LiFePO_4$ than it is for either the non-stoichiometric material or the carbon coated material. Actually the capacity limits of these latter two materials is nearly the same. At 20 C_{10}, 76% capacity is retained for both $LiFe_{0.9}P_{0.95}O_{4-\delta}$ and C/$LiFePO_4$, and only 65% is retained for the stoichiometric $LiFePO_4$. Again, the voltage curves of Fig. 8b reveal the source of the differences in performance. Whereas the three materials show about the same amount of initial voltage drop at the beginning of the discharge, additional impedance from limited solid state diffusion is apparent sooner in the stoichiometric material than the other two. This early onset of impedance results in reaching the 2.5 V cut-off limit in less time than the other two.

Also, compared with the rate performance of C/$LiFePO_4$ with 4.8% AB content, a great enhancement was observed for C/$LiFePO_4$ with 15% AB. Hence, the rate performance of the C/$LiFePO_4$ appears to be much more sensitive to AB content below 15% than the other two. The SEM images of Fig. 6 deserve a second look. For one, the C/$LiFePO_4$ electrodes with 4.8% AB appear brighter than the other two. This suggests that this material configuration lacks overall

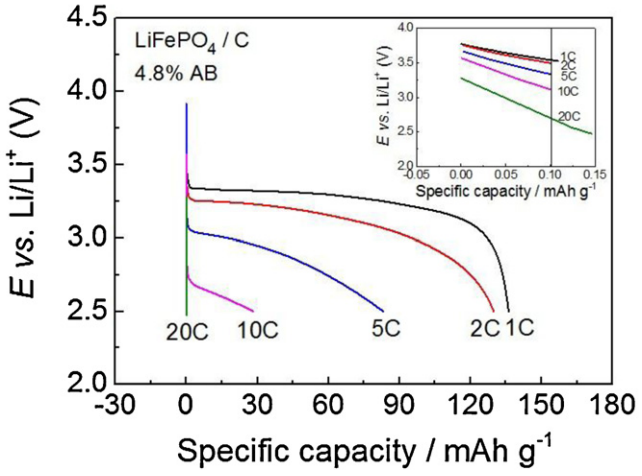

Fig. 9. The electrode potential plot of C/$LiFePO_4$ with 4.8% AB discharged at different currents.

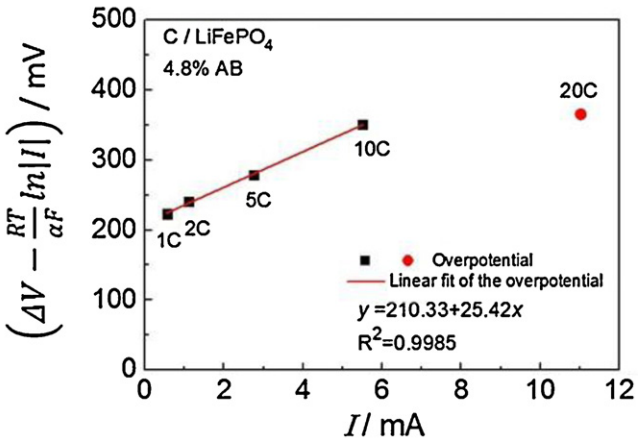

Fig. 10. The relationship of the overpotential with the electrode current.

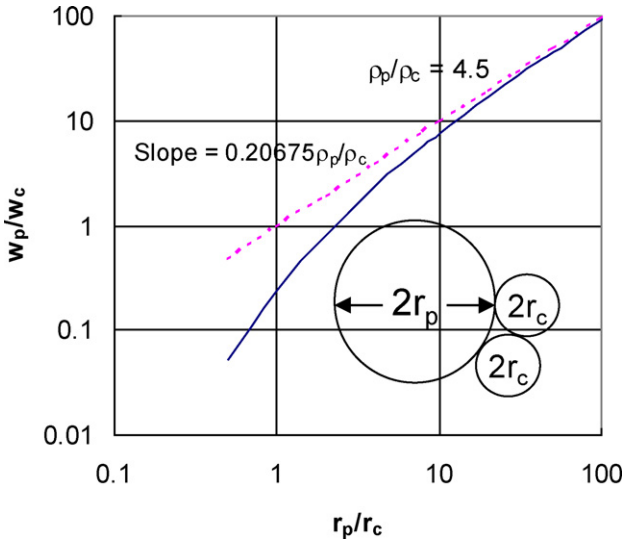

Fig. 11. Plot of w_p/w_c as a function of r_p/r_c.

conductivity. Also, the fairly smooth spheres appear much less connected to the AB. A model based on geometric arguments leads to Eq. (1), which was derived to calculate the amount AB required to completely cover a smooth, spherical particle:

$$\frac{w_p}{w_c} = b\left(\frac{\lambda}{1+(2/\lambda)+(1/\lambda^2)}\right) \quad (1)$$

where w_p is the weight percentage of the central particle (*i.e.* the active material), w_c is the weight percentage of the coating material (*i.e.* AB); $\lambda = r_p/r_c$, where r_p is the radius of center particle, r_c is the radius of the coating material, and $b = \rho_p/\rho_c \times 3\sqrt{3}/8\pi = \rho_p/\rho_c \times 0.20675$. ρ_p is the center particle's density (which is 3.6 g cm^{-3} for $LiFePO_4$) and ρ_c is the coating material density (which is 0.8 g cm^{-3} for compressed conductive AB when applied). If $\lambda = (400\,nm/50\,nm)$ and $\rho_p/\rho_c = 3.6/0.8$, then $w_c/w_p > 0.17$, which can also be read from the correlation plot in Fig. 11. This value is consistent with an electrode with 14% carbon, 81% $LiFePO_4$ and 5% binder. Thus, the 15% AB used in this test is just enough to cover all the active material in any of the three electrodes.

As the AB amount increases to 65% in the electrodes, more attention has to be paid to preparation of the laminate. To make a robust laminate, the AB, which arrives as a loosely packed network of strands of carbon, must be ball-milled to at least 30% of its original volume before addition to the slurry. For the $LiFe_{0.9}P_{0.95}O_{4-\delta}$ electrodes containing 65% AB, 70% of the capacity at $C_{10}/10$ is retained at 60 C_{10} when discharged to 2.5 V. This is consistent with that reported [14], even though the electrode fabrication method, the AB, and the binder used in the published report are different than those used here. Fast charge and discharge capability was also observed for the C/$LiFePO_4$: 60.5% of the capacity measured at $C_{10}/10$ is retained at 60 C_{10}. Such a result has never previously been reported for carbon-coated $LiFePO_4$ particles >100 nm. However, only 43% of the $C_{10}/10$ capacity was obtained at 60 C_{10} for the stoichiometric $LiFePO_4$.

In essence, the non-stoichiometric material that consists of amorphous, inorganic-coated, 25 nm particles that agglomerate into 100 nm secondary particles display the same ability to be discharged at rates exceeding 60 C_{10} mA as the carbon-coated, 100 nm, stoichiometric material. At these high carbon additive contents and low active material loadings, the electrodes' rate capabilities are solely limited by their solid-state diffusion. Fig. 12 shows the potential profiles of $LiFe_{0.9}P_{0.95}O_{4-\delta}$, stoichiometric $LiFePO_4$, and C/$LiFePO_4$ with 65% AB at $C_{10}/10$ and 60 C_{10}. At the low charge and

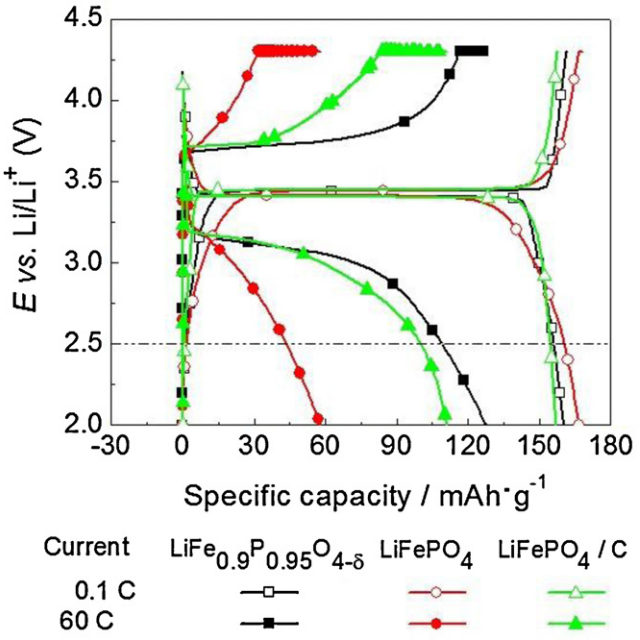

Fig. 12. The potential plots of $LiFe_{0.9}P_{0.95}O_{4-\delta}$, stoichiometric $LiFePO_4$ and C/$LiFePO_4$ with 65% AB at $C_{10}/10$ and 60 C_{10}. (The cells charged/discharged from 2 V to 4.3 V. The loading density of $LiFe_{0.9}P_{0.95}O_{4-\delta}$, stoichiometric $LiFePO_4$, and C/$LiFePO_4$ electrodes is 5.40, 4.91, and 4.17 mg cm^{-2}, respectively.)

discharge rate ($C_{10}/10$), the voltage plateaus of the three materials do not show very much ohmic or charge transfer polarization. As the cells reach the end of discharge, the voltage curve of the $LiFe_{0.9}P_{0.95}O_{4-\delta}$ and C/$LiFePO_4$ materials fall off sharply. For the stoichiometric $LiFePO_4$, the voltage of the cell starts to fall off a little sooner and more gradually than the other two materials. At this stage, it is not clear as to whether this is due to a difference in the open circuit voltage curve or due to a poorer solid state diffusion coefficient in this material at low states of charge. At the high discharge rate (60 C_{10}), one sees the effects of ohmic and/or charge transfer and Li^+ diffusion polarization for all three materials. The initial potential drop is similar for all three electrodes when the discharge is initiated. The difference between materials appears at longer times in the discharge – namely, the stoichiometric material has such poor mass transfer that it never levels off during the discharge but dives towards the lower cut-off voltage during most of the discharge. This performance is found independent of the active material loading, although all of the films are fairly thin, which leads us to believe that the source of this mass transfer limitation is the solid state diffusion of lithium in the active material.

With regard to the other two materials with coatings, they exhibit high rate capability with both 15% and 65% AB additive, with the $LiFe_{0.9}P_{0.95}O_{4-\delta}$ possessing slightly better rate capability despite the electronic conductivity of $LiFe_{0.9}P_{0.95}O_{4-\delta}$ being 8 orders of magnitude lower than that of C/$LiFePO_4$ (Fig. 5). Thus, it is clear that the electronic conductivity of these materials is not a key factor in governing the rate performance once enough carbon is added to entirely coat the active material. Thus, since the secondary particle sizes in the electrodes are nearly the same (Fig. 4 and Table 1), and the fabrication of the electrodes and cell tests were the same, the variations in performance must derive from the solid state Li^+ diffusion.

The Li^+ diffusion pathways of the three materials are depicted in Fig. 13, which helps to explain the difference in rate capability. Fig. 13a and b shows the primary particles of $LiFe_{0.9}P_{0.95}O_{4-\delta}$ and stoichiometric $LiFePO_4$, respectively, sintered together into secondary particles. The TEM of the particles leads us to believe that

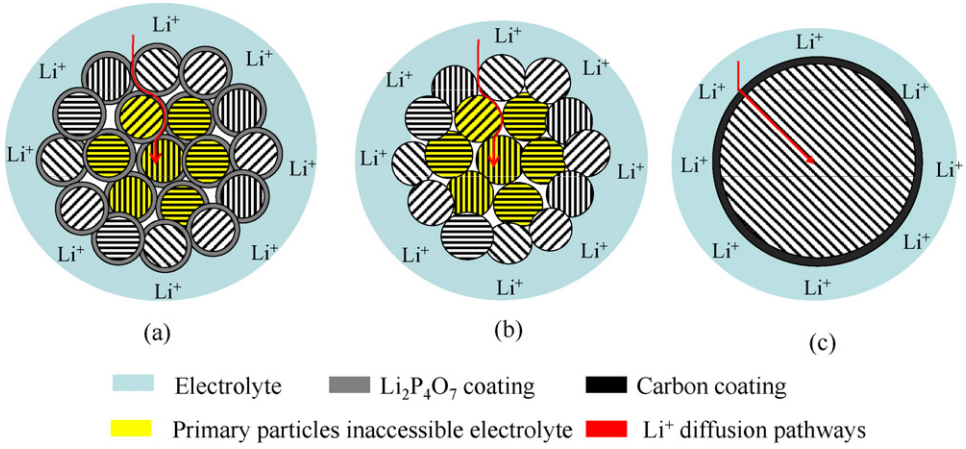

Fig. 13. Schematic illustration of Li^+ diffusion for different $LiFePO_4$ materials: (a) secondary particle of $LiFe_{0.9}P_{0.95}O_{4-\delta}$; (b) secondary particle of stoichiometric $LiFePO_4$; and (c) primary particle of C/$LiFePO_4$.

electrolyte is not able to penetrate the pores of the secondary particles. Thus, the Li^+ must find a solid diffusion path to reach the primary particles located at the center of a secondary particle. We believe that for the amorphous-coated nanoparticles (Fig. 13a), the coating offers higher diffusion rates for lithium than the diffusion down the 1-D tunnels of $LiFePO_4$; however this path is tortuous. In contrast, for the large, carbon-coated particles (Fig. 13c) the 1-D tunnels are the only a path to the center of the particle, but the path is non-tortuous. Apparently, these two alternatives offer roughly the same rate capability for discharging the material. On the other hand, the stoichiometric material has no high diffusion rate amorphous coating on the primary particles, and hence, the only path to the center of the secondary particles is a tortuous path *via* the 1-D tunnels.

4. Conclusions

In this study, carbon and amorphous, inorganic coated $LiFePO_4$ materials were prepared, characterized, and tested in Li half-cells. Stoichiometric nano-$LiFePO_4$ was also synthesized as the control using the same process by which the amorphous coated nano-$LiFePO_4$ material was produced. The particle sizes are in the same range for all three materials as assembled in an electrode. Although a difference of 8 orders of magnitude of electronic conductivity was found between the nano-$LiFePO_4$ materials and the carbon-coated $LiFePO_4$, they all possess fast charge and discharge capabilities if enough carbon additives are present. For the stoichiometric, nano-$LiFePO_4$, the rate performance is poorer than that of the other two $LiFePO_4$ materials. It is believed that the coated nanomaterial offers a fast, but tortuous path to the center of the secondary particle, the carbon coated $LiFePO_4$ offers a straight, but slow path to the center of the 100 nm size particles, and that the stoichiometric, nanomaterial offers tortuous, slow 1-D tunnels, and thus demonstrates the worst discharge performance of the three. When only 4.8% conductive carbon is present in the electrodes, the carbon coated material offers the worst performance. We believe this is a result of poor interaction between the additive and the active material surface, which may be due to higher binder loadings on the large, smooth C/$LiFePO_4$ crystals and the conductive additive, leading to contact resistance and poor charge transfer.

Acknowledgements

This research is funded by the Assistant Secretary for Energy Efficiency, Office of Vehicle Technologies of the US Department of Energy as part of the BATT program under Contract No. DE-AC02-05CH11231. The authors thank Dr. Karim Zaghib from the Institute de Recherché d'Hydro-Québec (IREQ) for providing C/$LiFePO_4$ sample and thank Professor G. Ceder and Dr. B.W. Kang (MIT) for their support in the synthesis of $Li_4P_2O_7$ coated $LiFePO_4$ sample. The National Center for Electron Microscopy at LBNL is acknowledged for the TEM experiments.

References

[1] A.K. Padhi, K.S. Nanjundaswamy, J.B. Goodenough, J. Electrochem. Soc. 144 (1997) 1188.
[2] A.K. Padhi, K.S. Nanjundaswamy, C. Masquelier, S. Okada, J.B. Goodenough, J. Electrochem. Soc. 144 (1997) 1609.
[3] N. Ravet, J.B. Goodenough, S. Besner, M. Simoneau, P. Hovington, M. Armand, Abstract # 127, in: 196th Meeting of the Electrochemical Society, Hawaii, 1999.
[4] H. Huang, S.C. Yin, L.F. Nazar, Electrochem. Solid-State Lett. 4 (2001) A170.
[5] Z.H. Chen, J.R. Dahn, J. Electrochem. Soc. 149 (2002) A1184.
[6] R. Dominko, M. Bele, M. Gaberscek, M. Remskar, D. Hanzel, S. Pejovnik, J. Jamnik, J. Electrochem. Soc. 152 (2005) A607.
[7] K. Zaghib, P. Charest, M. Dontigny, A. Guerfi, M. Lagace, A. Mauger, M. Kopec, C.M. Julien, J. Power Sources 195 (2010) 8280.
[8] Y. Cui, X.L. Zhao, R.S. Guo, J. Alloys Compd. 490 (2010) 236.
[9] Y. Cui, X.L. Zhao, R.S. Guo, Mater. Res. Bull. 45 (2010) 844.
[10] H.H. Chang, C.C. Chang, C.Y. Su, H.C. Wu, M.H. Yang, N.L. Wu, J. Power Sources 185 (2008) 466.
[11] H. Liu, G.X. Wang, D. Wexler, J.Z. Wang, H.K. Liu, Electrochem. Commun. 10 (2008) 165.
[12] G.M. Song, Y. Wu, G. Liu, Q. Xu, J. Alloys Compd. 487 (2009) 214.
[13] G.M. Song, Y. Wu, Q. Xu, G. Liu, J. Power Sources 195 (2010) 3913.
[14] B. Kang, G. Ceder, Nature 458 (2009) 190.
[15] K. Zaghib, J.B. Goodenough, A. Mauger, C. Julien, J. Power Sources 194 (2009) 1021.
[16] G. Ceder, B. Kang, J. Power Sources 194 (2009) 1024.
[17] J.J. Chen, M.S. Whittingham, Electrochem. Commun. 8 (2006) 855.
[18] H. Zheng, G. Liu, S. Crawford, V. Battaglia, http://berc.lbl.gov/vbattaglia/cell-analysis-tools/sss.
[19] P.S. Herle, B. Ellis, N. Coombs, L.F. Nazar, Nat. Mater. 3 (2004) 147.
[20] K.F. Hsu, S.Y. Tsay, B.J. Hwang, J. Mater. Chem. 14 (2004) 2690.
[21] J. Sanchez-Gonzalez, A. Macias-Garcia, M.F. Alexandre-Franco, V. Gomez-Serrano, Carbon 43 (2005) 741.
[22] A. Awarke, S. Lauer, S. Pischinger, M. Wittler, J. Power Sources 196 (2011) 405.